

Article

Simplified Model of a High Burnup Spent Nuclear Fuel Rod under Lateral Impact Considering a Stress-Based Failure Criterion

Seyeon Kim and Sanghoon Lee *

Department of Mechanical Engineering, Keimyung University, Daegu 42601, Korea; syeonkim@stu.kmu.ac.kr
* Correspondence: shlee1222@kmu.ac.kr; Tel.: +82-53-580-5264; Fax: +82-53-580-5165

Abstract: The inventory of spent nuclear fuel (SNF) generated in nuclear power plants is continuously increasing, and it is very important to maintain the structural integrity of SNF for economical and efficient management. The cladding surrounding nuclear fuel must be protected from physical and mechanical deterioration, which causes fuel rod breakage. In this study, the material properties of the simplified beam model of a SNF rod were calibrated for a drop accident evaluation by considering the pellet–clad interaction (PCI) of the high burnup fuel rod. In a horizontal drop, which is the most damaging during a drop accident of SNF, the stress in the cladding caused by the inertia action of the pellets has a great effect on the integrity of the fuel rod. The failure criterion for SNF was selected as the membrane plus bending stress through stress linearization in the cross-sections through the thickness of the cladding. Because the stress concentration in the cladding around the vicinity of the pellet–pellet interface cannot be simulated in a simplified beam model, a stress correction factor is derived through a comparison of the simplified model and detailed model. The applicability of the developed simplified model is checked through dynamic impact simulations. The developed model can be used in cask level analyses and is expected to be usefully utilized to evaluate the structural integrity of SNF under transport and in storage conditions.

Keywords: spent nuclear fuel; high burnup fuel; simplified model; calibration; degradation characteristics; stress linearization; membrane plus bending stress; stress correction factor; pellet–clad interfacial bonding condition; finite element analysis



Citation: Kim, S.; Lee, S. Simplified Model of a High Burnup Spent Nuclear Fuel Rod under Lateral Impact Considering a Stress-Based Failure Criterion. *Metals* **2021**, *11*, 1631. <https://doi.org/10.3390/met11101631>

Academic Editor: Robert W. Harrison

Received: 13 September 2021

Accepted: 7 October 2021

Published: 14 October 2021

Publisher's Note: MDPI stays neutral with regard to jurisdictional claims in published maps and institutional affiliations.



Copyright: © 2021 by the authors. Licensee MDPI, Basel, Switzerland. This article is an open access article distributed under the terms and conditions of the Creative Commons Attribution (CC BY) license (<https://creativecommons.org/licenses/by/4.0/>).

1. Introduction

The spent nuclear fuel (SNF) discharged from a nuclear reactor is stored for several years to decades in wet storage and at an interim storage facility (ISF) for cooling before reprocessing or direct disposal [1]. The storage of SNF is consistently increasing worldwide, and dry storage facilities are operated in preparation for the saturation of wet storage [2]. It is essential that the SNF maintains a handleable condition without damage to the nuclear fuel rods before the final disposal or reprocessing. For this purpose, it is necessary to keep the structural integrity of the nuclear fuel rods from deteriorating, which could cause extensive damage to the cladding during the storage period [3–5]. Structural analysis using CAE (computer aided engineering) is important, but a single SNF cask contains dozens of fuel assemblies and thousands of fuel rods. Accordingly, the total number of elements of a transportation or storage cask is impractical if all the details of the fuel assemblies are to be modeled. The uncertainties lying in the physical-mechanical properties of SNF pose more difficulties to the structural evaluation of SNF. Choi et al. [6] verified the conditions under which delayed hydride cracking could occur for the integrity evaluation of the effect of hydride on the cladding during dry storage of SNF and compared the critical loads of delayed hydride cracking for the cladding with different hydrogen contents. In accordance with safety regulations, fuels must be protected from deterioration in physical–mechanical properties, resulting in damage to nuclear fuels [7,8]. However, even if the characteristics

of SNF and the burnup are defined, the properties of SNF are uncertain when exposed to high temperatures and irradiation environments in a nuclear reactor. Jiang et al. [9,10] performed an extensive study on the impact of pellet-cladding interaction (PCI) on the fuel rod performance. Almomani et al. [11] studied the behavior of fuel rods about their buckling and bending resistance in drop accidents, using the properties of SNF and PCI as parameters, and recently analyzed the importance of the PCI on the structural integrity of SNF [12]. Lee et al. [13] studied the calibration of the simplified beam model properties of SNF by considering the PCI. However, these simplified model properties calibrated at a specific segment length as a reference have a large dependence on the length of the fuel rod being considered, showing that its applicability is limited. Thus, Lee and Kim [14] developed a new simplified model that was not limited by the length of the reference fuel rod segment.

In this study, a simplified model was developed for the horizontal drop condition, where the characteristics of the bending resistance of the fuel rods are dominant. It is known that this drop orientation is the most damaging to fuel rods. A new cladding failure criterion is proposed, which is based on linearized stress distribution through the thickness of the cladding. This criterion can account for the localized stress concentration and the through-thickness development of stress from which cladding failure can occur. The optimization for material property calibration of the simplified model was performed based on this stress-based criterion for two extreme interfacial conditions. The two extreme conditions are as follows: (1) a fully de-bonded condition is a gap between the pellets and the cladding when SNF was first stored, and (2) a fully bonded condition is where the pellets and the cladding are bonded through a physical–chemical reaction over time due to high temperatures and high pressures. To calibrate the properties of the simplified beam model, optimization of the properties of the simplified model is performed for the structural response of the detailed fuel rod model, using the equation of the same elastic–plastic material as that of the Zircaloy-4 cladding. Development of the simplified model proceeds in four stages. The first is to select the interfacial bonding condition among the degradation characteristics of the SNF; the second is to analyze the fuel rod mechanical behaviors; the third is to develop a simplification model; and finally, an applicability test is conducted on the developed simplified model.

2. Material Model for the Target Fuel Rod

2.1. Target Fuel Rod

The design of the fuel rod assembly considered in this study refers to the CE 16 by 16 assembly model in Figure 1, and the design specifications are shown in Table 1. A nuclear fuel rod consists of fuel pellets and Zircaloy-4 cladding surrounding it. In a fresh fuel rod, there exists a small gap between the pellets and the cladding, but during reactor operation with high burnup, the gap is filled with a fused material or compressed through residual stress caused by the mechanical interaction of the two interfaces. Because the pellet–cladding interface (PCI) has a strong influence on the dynamic response of SNF, two extreme interfacial conditions were considered in this study. The target fuel rod considered in this study was a high burnup fuel (HBF) with a burnup rate of over 45 GWd/MTU.

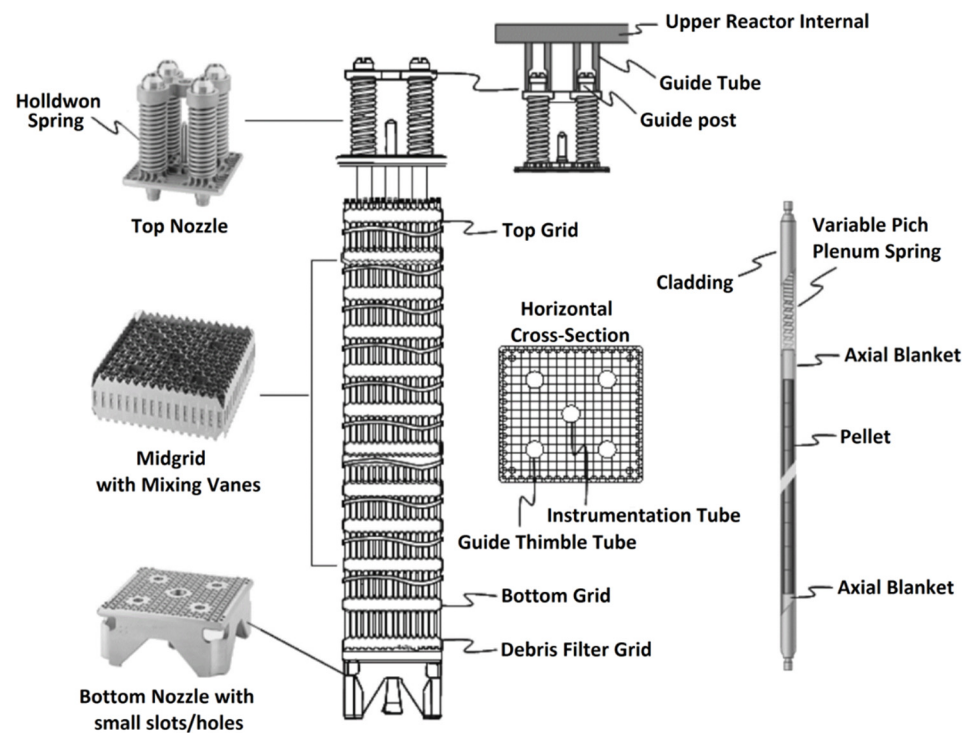


Figure 1. CE 16×16 fuel assembly design feature of the PLUS7. Reprinted with permission from ref. [15].

Table 1. Specifications of the fuel rod and assembly considered. Reprinted with permission from ref. [11].

Parameter	Value
Cladding length (L)	4.094 m
Outer diameter of cladding (OD) (r_o)	4.75 mm
Inner diameter of cladding (ID) (r_i)	4.178 mm
Diametral gap	165 μ m
Distance between two sequent spacer grids	396.9 mm
Area moment of inertia of the cladding (I_c)	160.508 mm ⁴
Area moment of inertia for the pellet (I_p)	239.291 mm ⁴
Pellets diameter	8.191 mm
Pellets length	11.34 mm
Number of pellets in full fuel rod	350
Pellets hollow depth	0.3 mm
Pellets hollow radius	14 mm
Pellets hollow apparent radius	2.95 mm
Pellet edge chamfer radius	3.55 mm
Pellets edge chamfer depth	0.16 mm
Gap With adjacent pellets	No gap
Total weight of single rod (W)	2.58 kg
Fraction of theoretical density of UO ₂ (%TD)	95%
Assembly weight	639 kg
Number of rods	236
Number of spacer grids	12

2.2. Material Model of the Degraded HBF Cladding and Pellets

The properties of the HBF are functions of parameters such as the burnup and storage conditions, and important factors that influence the HBF properties include the hydrogen concentration, irradiation level, and temperature. Based on much experimental data, a detailed model was developed to predict the mechanical properties of the pellets and

cladding as functions of the temperature, neutron fluence, hydrogen content, and burnup [16,17]. In this study, the parameters of the fuel were as follows: a discharge burnup of 60 GWd/MTU, a temperature of 573 K corresponding to a 5 year dry storage condition, a neutron fluence of 11.4×10^{25} n/m², and a total hydrogen concentration of 352 ppm. A detailed explanation about the choice of the above parameters can be found in [11]. The cladding material is described as an elastoplastic material that can be mathematically formulated using Hook's law and power law, as in following equations:

$$\sigma_y = \left[KE^{-n} (1000\dot{\epsilon})^m \right]^{\left(\frac{1}{1-n}\right)}, \quad (1)$$

$$\sigma_{e+p} = UE + \sigma_y E^{-n}, \quad (2)$$

where σ_y is the yield stress (MPa); K is the strength coefficient; E is Young's modulus (MPa); n is the strain hardening exponent; m is the strain rate exponent; $\dot{\epsilon}$ is the strain rate(/s); σ_{e+p} is the true stress; and UE is the uniform elongation. The parameters in the model for the reference fuel rods considered in this study are summarized in Table 2. At 573 K, with only circumferential hydride, the fracture strain of the target HBF Zircaoly-4 cladding is known to be 1~4% [18], and the failure stress corresponding to a 1% plastic strain is 749 MPa. In this study, a stress of 749 MPa was selected as the failure criterion of the fuel cladding [19,20].

Table 2. Mechanical parameters of the fuel rod model. Reprinted with permission from ref. [11].

Parameters	Mechanical Properties
1. Zircaloy cladding (SRA Zry-4)	
a. Mass density (ρ_c)	6590 kg/m ³
b. Modulus of elasticity (E)	75.22 GPa
c. Strength coefficient (K)	14.43 GPa
d. Strain hardening exponent (n)	0.159
e. Strain rate exponent (m)	0.015
f. Shear modulus (G)	28.28 GPa
g. Poisson's ratio (ν)	0.33
h. Uniform plastic elongation (UE)	0.022
i. Yield strength (σ_y)	644.79 MPa
j. Ultimate tensile strength (σ_{e+p})	788.68 MPa
2. Fuel (uranium dioxide (UO ₂))	-
a. Mass density (ρ_p)	10,440 kg/m ³
b. Modulus of elasticity (E)	168.3 GPa
c. Poisson's ratio (ν) *	0.32
d. Yield strength (σ_y) *	2146 MPa

2.3. Determination of the Failure of the Fuel Cladding

The failure strain of irradiated Zircaloy-4 cladding was obtained by experimental measurement using the uniaxial tension test or pressurized tube test with defueled cladding specimens. In both tests, an almost uniform tensile stress and strain are induced through the thickness of the cladding. This stress state and deformation pattern are quite different from those observed in actual fuel rods with fuel pellets. When a fuel rod is subject to bending, a very complicated 3D stress state is generated within the vicinity of the pellet-pellet interface shown in Figure 2. A very localized stress concentration is observed in the area where the edges of the pellets contact the cladding. If the failure strain criteria obtained from the uniaxial tension test or biaxial tube test is applied, very early failure is predicted at the beginning stage of loading with premature through-thickness stress or strain development. The localized contact stress or strain is self-limiting and is not a good candidate for the cladding failure criteria.

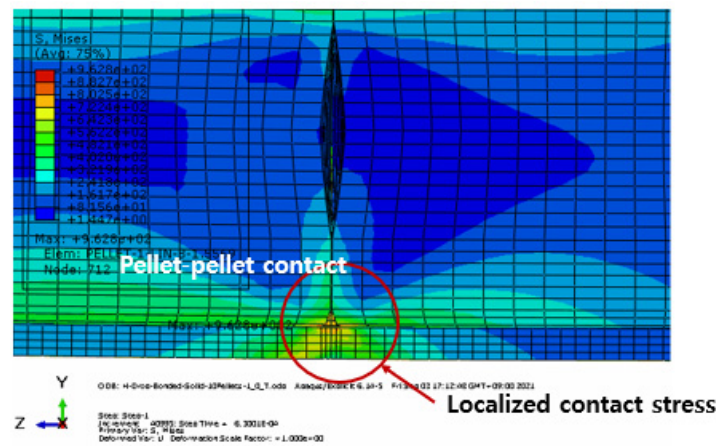


Figure 2. Effect of the pellet–pellet contact and pellet–clad interaction on the cladding strain.

Therefore, a new cladding failure criterion is proposed in this work, which can account for the localized stress concentration and the through-thickness stress development. The failure of the cladding is determined by the membrane plus bending stress generated through the thickness of the cladding, which can be calculated by a process called stress linearization along the stress classification line shown in Figure 3. The fuel rod failure criterion was based on the aforementioned stress of 749 MPa of the membrane plus bending contribution of the von Mises stress of the cladding.

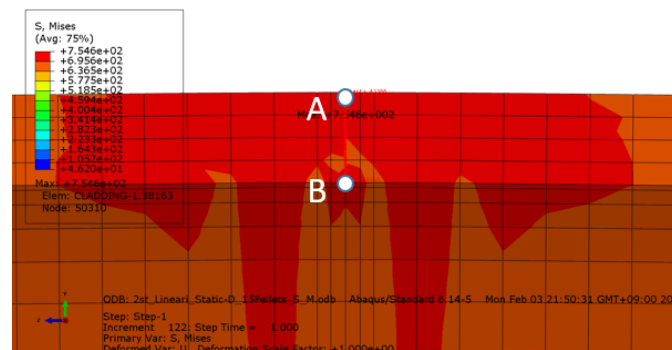


Figure 3. Stress linearization through the thickness of the cladding.

Stress linearization is a process of decomposing the total stress generated in an arbitrary cross-section of a structure into three stress components, as shown in Figure 4, and evaluated by linearizing the stress distribution in the thickness direction of the structure [21]. The membrane values of the stress components are computed using Equation (3), and it does not transfer any moments. Assuming that the whole thickness between point A and point B in Figure 5 are divided uniformly into n intervals, the thickness membrane stress can be calculated as the average thickness stress by solving Equation (4). The linear bending values of the stress components at the endpoints of the sections are computed using Equation (5), and thickness surface stress does not have a peak stress contribution. Hence, the thickness bending stress is that of the sum of the thickness membrane and bending stresses at the total stress at each point, as shown in Equation (6), and interpolates the bending stress linearly [22,23].

$$\sigma^m = \frac{1}{t} \int_{-t/2}^{t/2} \sigma dx, \quad (3)$$

$$\sigma_t^m = \frac{1}{2n} \sum_{j=1}^n (\sigma_{t(j)} + \sigma_{t(j+1)}), \quad (4)$$

$$\sigma_A^b = -\sigma_B^b = \frac{6}{t^2} \int_{-t/2}^{t/2} \sigma \cdot x \cdot dx, \quad (5)$$

$$\sigma_{tA}^b = \sigma_{tA} - \sigma_t^m, \quad \sigma_{tB}^b = \sigma_{tB} - \sigma_t^m, \quad (6)$$

where σ^m is the membrane stress (MPa); t is the thickness of the section; σ is the stress along the path; x is the coordinate along the path; and n is the uniform intervals divided between endpoints. In Equation (5), σ_A^b and σ_B^b are the bending stress at the endpoints of the section in Figure 3. σ_{tA} and σ_{tB} are the total thickness stress at the endpoints A and B.

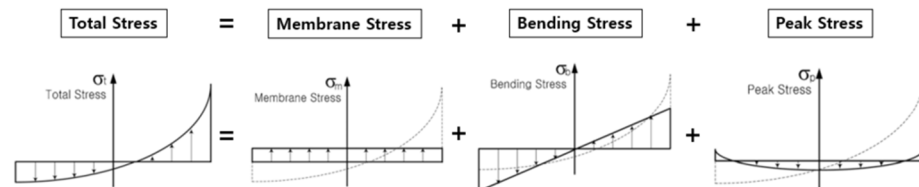


Figure 4. Decomposition of the linear stress distribution. Reprinted with permission from ref. [21].

3. Development of the Simplified Beam Model of a SNF Rod under Pure Bending

3.1. Strategy of the Model Simplification

The purpose of developing the simplified model is to develop a fuel rod model that can be used in transport or storage cask analyses to evaluate the structural integrity of nuclear fuel rods and to calculate the fuel damage ratio under accident conditions. During the cask drop impact, the fuel rods receive the inertial load from the impact acceleration and the pinch loads that occur due to collision with other fuel rods and the baskets in the cask. In the work of Lee and Kim [14], a simplified model was developed that considered the deflection of the fuel rods under a pure bending moment, and it was demonstrated that the simplified beam model is not dependent on the length of the reference fuel rod segment for calibration. A 1% plastic strain calculated from the curvature of the fuel rod was used as the failure criterion of the cladding. However, this criterion cannot account for the effect of the localized stress concentration in the vicinity of the pellet–pellet interface, which obviously promotes the failure of the cladding.

In this work, the framework of the model calibration proposed by Lee and Kim [14] is modified using a new cladding failure criterion. The strategy of the model calibration is as follows: (1) the fuel rod is simplified into a hollow beam with an isotropic material; (2) the flexural rigidity of the simplified beam should be matched with that of the detailed model so that the deflection and pinch load can be estimated accurately; (3) because an isotropic beam cannot express the localized contact stress, a factor named the stress correction factor is proposed so that the same failure criterion can be applied to the simplified model.

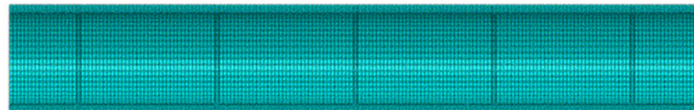
To implement a model calibration procedure that complies to the above-mentioned strategy, a reference fuel rod segment of 56.7 mm in length was chosen, and the critical bending moment was calculated using static analyses with the detailed model. The critical bending moment is the one that produces 749 MPa of membrane plus bending stress through a thickness of the cladding. The parameters of the simplified beam were calibrated in such a way that the deflection of the simplified model is matched with that of the detailed model under this critical bending moment. This procedure is applied to the fully bonded fuel rod and fully de-bonded fuel rod separately to account for the effect of the PCI.

3.2. Detailed Finite Element Model and Results of the Static Analyses

The detailed fuel rod model used in this study is shown in Figure 5. A half model of a fuel rod segment was constructed using the symmetry condition. A total of 24,768 elements of an eight-node linear brick and incompatible modes were used in this model. To see the stress distribution between the inner surface of the cladding contacting the corner of the pellets in detail, a dense mesh was used in the corresponding cladding area shown in Figure 6. In the fully bonded condition, the outer surface of the pellets and the inner

surface of the cladding were given the tie constraints, and the fully de-bonded condition was simulated using the frictionless contact conditions. The detailed modeling conditions for the two interfacial conditions are shown in Table 3. The bending moment applied to a fuel rod is given in Figure 7. A more detailed explanation of interfacial bonding and its effect can be found in [9,10]. The hoop stress distribution caused by the rod internal pressure was not considered in this work. It can be obtained using code such as FRAPCON [24] and will be investigated in our future work.

▪ **Part 1 : Cladding**



▪ **Part 2 : Pellet**

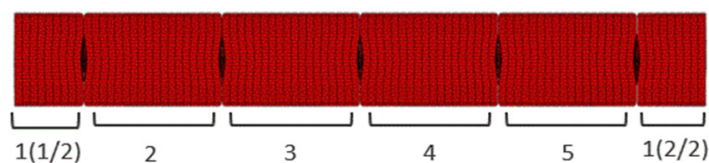


Figure 5. Detailed fuel rod segment model of 56.7 mm.

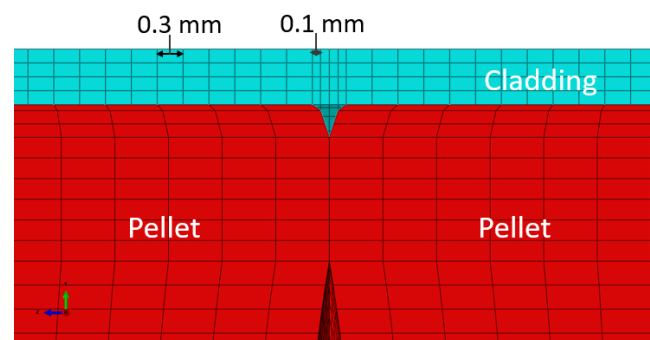


Figure 6. Mesh density of the cladding.

Table 3. Interfacial bonding condition modeling of the fully bonded and de-bonded conditions.

Interfacial Bonding Condition	Interface	Modeling
Fully bonded	Pellet–Pellet Pellets–Cladding	Frictionless hard contact Tie constraints
Fully de-bonded	Pellet–Pellet Pellets–Cladding	Frictionless hard contact Frictionless hard contact

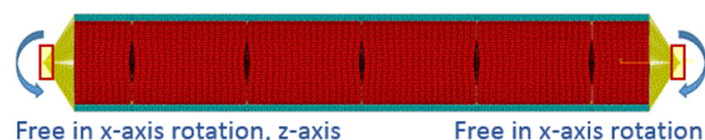


Figure 7. Constraints of the detailed fuel rod.

Static analyses for the two interfacial bonding conditions were performed, and the critical moment that generates a membrane plus bending stress of 749 MPa through the thickness of cladding was derived using linear interpolation. The results of the moment at which the failure occurs are 31,413 N·mm for the fully bonded condition and 22,410 N·mm for the fully de-bonded condition. The deformed shapes and stress linearization are shown in Figure 8.

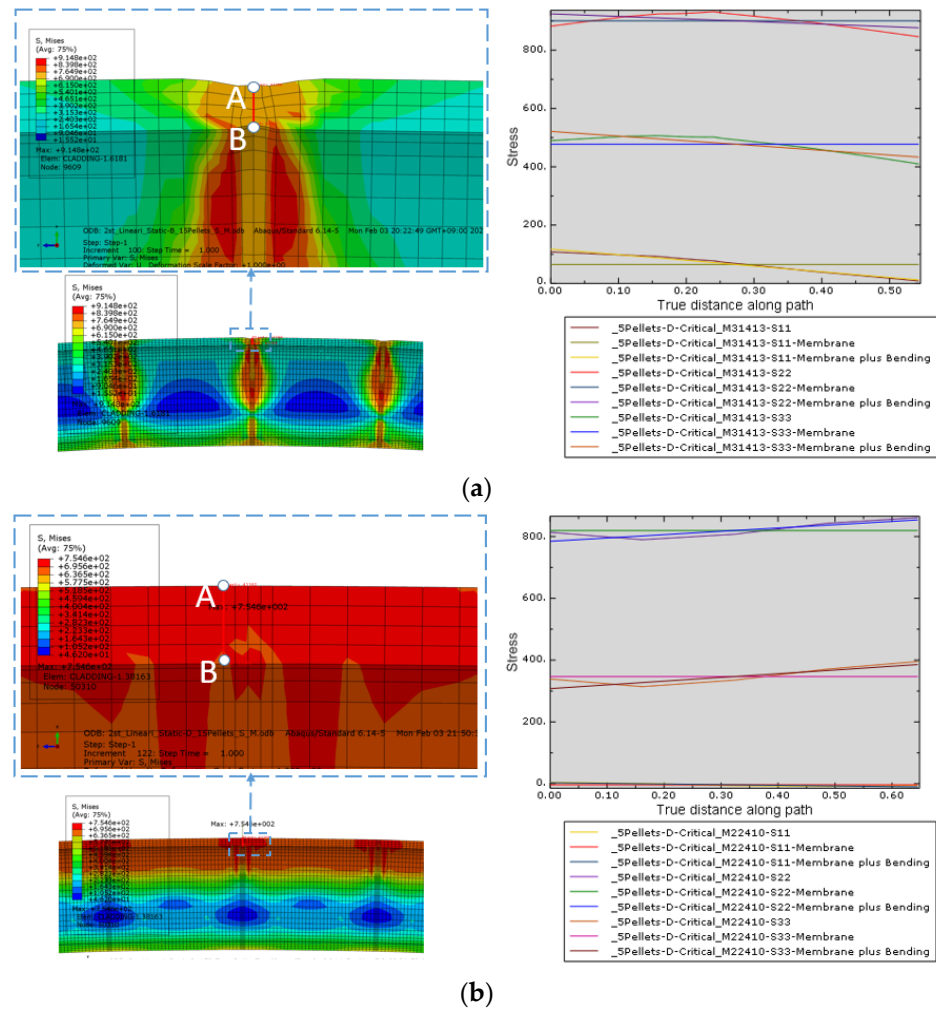


Figure 8. Stress linearization for the critical bending moment results of the detailed models: (a) stress linearization results of the fully bonded condition detailed model; (b) stress linearization results of the fully de-bonded condition detailed model.

In the work of Lee and Kim [14], the critical bending moments were calculated from the curvature of the fuel rods, and they were 31,919 N·mm for the fully bonded case and 27,975 N·mm for the fully de-bonded case. It was observed that the failure criterion used in this work predicts almost the same critical moment for the fully bonded fuel rods, while smaller critical moments are predicted for the fully de-bonded case. This result implies that the linearized stress-based criterion of this work takes more account of the localized stress compared to the curvature-based criteria of [14].

3.3. Parameter Calibration for the Simplified Model

The material of the simplified model was modeled as an elastic–plastic material described with the same equation used for Zircaloy-4 in Section 2. Young’s modulus of the simplified model was calculated using Equation (7) with the analyses results of the detailed model as follows:

$$E_s = \frac{1}{8} \cdot \frac{ML^2}{I} \cdot \frac{1}{\delta_d'} \quad (7)$$

where E_s is Young’s modulus of the simplified beam model (GPa); M is the bending moment (N·mm) of a small, arbitrary value under which the fuel rod shows a linear behavior; L is the length of the fuel rod segment (mm); I is the area moment of the inertia for the simplified beam model (mm⁴); and δ_d' is the vertical deflection of the detailed

fuel rod under M . The area moment of the inertia I is determined from the calibration parameters, and as a result, the E_s also varies with the choice of calibration parameters.

For the calibration of the properties of the simplified beam model, ISGITH [25], the optimization program, was used to optimize the calibration parameters to minimize the discrepancy in the behavior of the simplified model and the detailed model. The strength coefficient (MPa), the strain hardening exponent n , and the thickness of the hollow shaft beam T were considered as the parameters of the calibration. The calibration procedure was formulated into an optimization problem as follows:

$$\begin{aligned} & \text{Find } K, n \text{ and } T \text{ such that} \\ & \text{Minimize } (U_{E_d} - U_{E_s})^2 + (U_{C_d} - U_{C_s})^2, \end{aligned} \quad (8)$$

where U_E is the displacement of the fuel rod in the elastic region, and U_C is the displacement of the fuel rod under the critical moment. The subscripts d and s denote the detailed model and the simplified model, respectively. The optimization procedure is depicted in Figure 9.

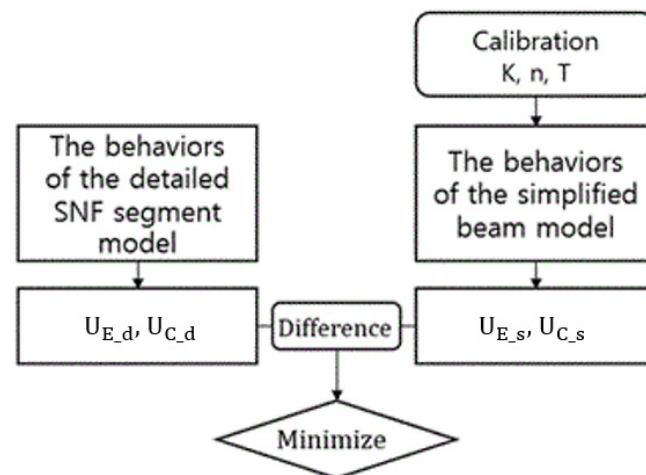


Figure 9. Optimization formulation of the simplified beam model.

The structural response of the simplified beam model was calculated using the ABAQUS/Standard (V2016, Dassault Systèmes Simulia Corp, Warwick, RI, USA). Using MATLAB (R2016, Mathworks, Natick, MA, USA), the stress–strain relationship model is created by inputting the Zircaloy-4 property equation and calibration parameters K , n , and T . The material properties model is then inputted into the ABAQUS material table, and the displacement of the simplified model required for calculating the optimization objective functions is calculated. The displacement output is the input to the ISIGTH, and the design variables are updated until the objective function is minimized through the adaptive simulated annealing (ASA) method [26]. A total of 2,784 iterations for the fully bonded condition and 242 iterations for the fully de-bonded condition were performed before optimal solutions were obtained. The optimization results corresponding to each PCI condition are shown in Table 4. The material model derived through the optimized design variables was applied to the simplified model, and the deformed shape of the detailed model and the simplified model are compared in Figure 10. Figure 11 shows the moment–displacement curve. It is shown that the deflection of the simplified models agrees well with those of the detailed models at the evaluation points (U_E , U_C), although a slight discrepancy is observed in the plastic region. In the comparison of the membrane plus bending stress of the von Mises stress in the simplified model, which is the fuel rod failure criterion of the detailed model proposed in this study, it has a deviation of 44% in the fully bonded condition and 67% in the fully de-bonded condition. An idealized Euler beam cannot express the localized stress concentration observed in actual fuel rods, and this discrepancy in the stress was predictable. In this study, the error ratio was used to

calculate the stress correction factor to compensate for the stress results in the simplified models. Before that, it is necessary to check whether the von Mises stress result of the simplified model has a consistent error ratio for the various segment lengths in the two interface bonding conditions for the failure criterion of 749 MPa.

Table 4. Results of the beam model parameter calibration.

Interfacial Bonding Condition	Optimal Parameter Values			Critical Moment	U_{E_s} (dev.)	U_{C_s} (dev.)	σ_{vm}	
	K (GPa)	n	T (mm)				Value (MPa)	(dev.)
Fully bonded	2.180	0.359	1.23	31.4 N·m	0.357 (0.0%)	1.605 (1.0%)	422	44%
Fully de-bonded	1.888	0.415	1.68	22.4 N·m	0.390 (0.4%)	1.113 (0.0%)	245	67%

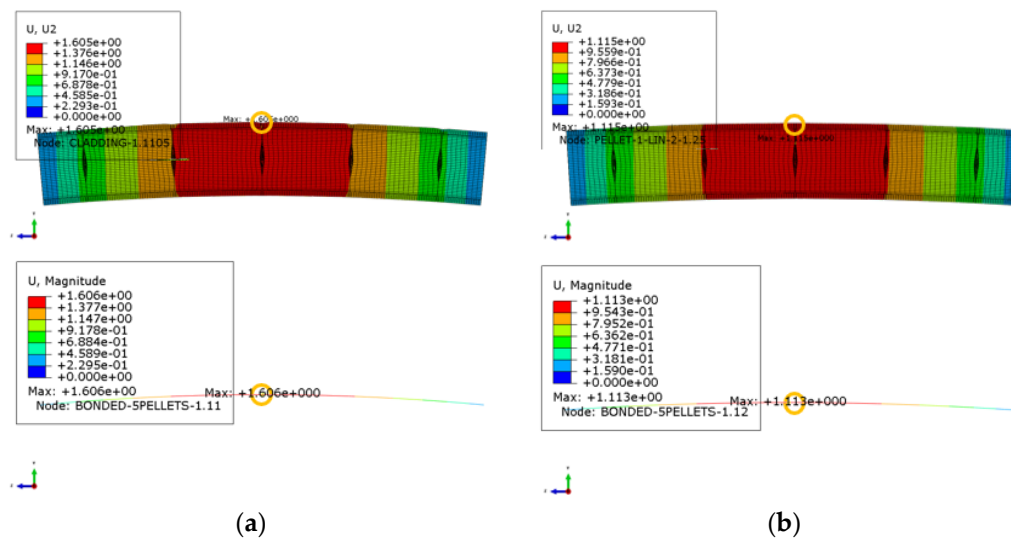


Figure 10. Deform shape for the critical moment of the detailed model and simplified model: (a) fully bonded condition; (b) fully de-bonded condition.

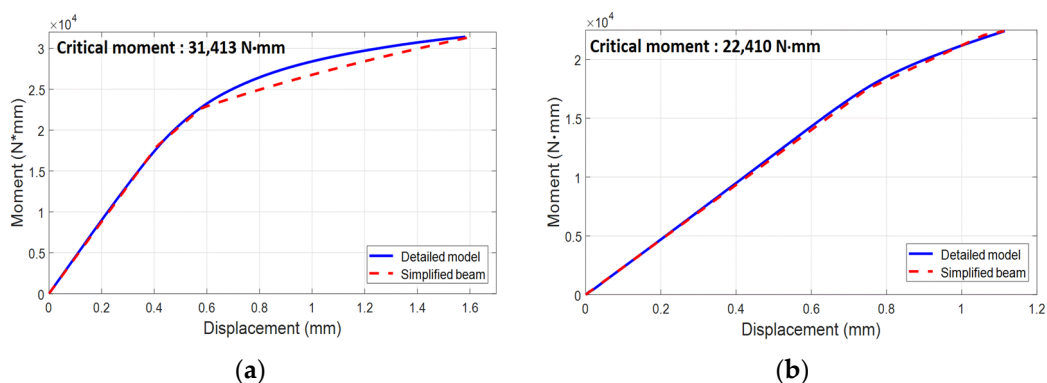


Figure 11. Moment–displacement characteristics of the detailed model and simplified model: (a) fully bonded condition; (b) fully de-bonded condition.

3.4. Discussions on the Failure Limit Criteria of the Cladding with Various Segment Lengths

A simplified model considering the bending load was developed for a fuel rod segment with a length of 56.71 mm containing five fuel pellets. The detailed and simplified models of five fuel rod segments with different lengths were constructed and analyzed to investigate whether the calibrated material parameters and error ratio are applicable to fuel rods

with different lengths. The beam parameters found in Section 3.3 were applied to all the simplified models. The 749 MPa membrane plus bending stress selected as the failure criterion at the critical moment and displacement of a simplified model with isotropic materials was compared for the two interfacial bonding conditions and summarized in Tables 5 and 6.

Table 5. Application of the simplified model parameters for the bonded condition to different lengths of fuel rod segments.

Cases	Number of Pellets	Length (mm)	Critical Moment (N·mm)	Model	Displacement (U_C)		Stress ($\sigma^m + \sigma^b, \sigma_{vm}$)	
					Value (mm)	Dev. (%)	Value (MPa)	Dev. (%)
1	5 (reference)	56.7	31,413	Detailed	1.58	1.0	749	44
				Simplified	1.61		422	
2	10	113.4		Detailed	5.84	0.6	749	44
				Simplified	5.87		423	
3	15	170.1		Detailed	12.98	1.9	751	44
				Simplified	12.74		423	
4	20	226.8		Detailed	22.04	0.5	747	44
				Simplified	21.16		423	
5	25	283.5		Detailed	34.50	1.8	752	44
				Simplified	33.88		423	
6	30	340.2		Detailed	48.85	1.2	752	44
				Simplified	48.28		423	

Table 6. Application of the simplified model parameters for the de-bonded condition to different lengths of fuel rod segments.

Cases	Number of Pellets	Length (mm)	Critical Moment (N·mm)	Model	Displacement (U_C)		Stress ($\sigma^m + \sigma^b, \sigma_{vm}$)	
					Value (mm)	Dev. (%)	Value (MPa)	Dev. (%)
1	5 (reference)	56.7	22,410	Detailed	1.11	0	749	67
				Simplified	1.11		245	
2	10	113.4		Detailed	3.97	2.9	749	67
				Simplified	4.09		245	
3	15	170.1		Detailed	8.64	2.9	750	67
				Simplified	8.90		245	
4	20	226.8		Detailed	15.04	3.1	749	67
				Simplified	15.52		245	
5	25	283.5		Detailed	23.19	3.1	749	67
				Simplified	23.93		245	
6	30	340.2		Detailed	33.02	3.1	749	67
				Simplified	34.09		245	

The structural response of the segments with various lengths shows almost identical deviation levels in both interfacial bonding conditions. At the critical moment, the maximum displacement deviation of the detailed model and the simplified model was 1.8% in the fully bonded condition and 3.1% in the fully de-bonded condition. When comparing

the membrane plus bending stress, the fully bonded condition showed a consistent 44% deviation, and the fully de-bonded condition showed a consistent 68% deviation. Thus, it is shown that the correlation of the behavior of models as well as the deviation percentages in the linearized stress are insensitivity to the choice of the length of the reference fuel rod segment for calibration. From this result, it was confirmed that the error ratio of 44% and 68% can be used to find the stress correction factor to compensate the stress calculation results using the simplified beam model, regardless of the lengths of the fuel rods being considered. The stress correction factor of the simplified model for the fully bonded condition is 1.78 and 3.06 for the fully de-bonded condition. It should be noted that these factors are applicable only to the fuel rods with the same specification with the one in the current study, which is subject to pure bending. The applicability of these factors and the factors those have effects on them will be investigated in our future study.

4. Applicability of the Developed Models in Dynamic Impact Simulations

4.1. Models for Impact Simulation and Impact Conditions

Dynamic impact simulations were performed using the detailed models and simplified models of fuel rods to check the applicability of the calibrated beam parameters. The procedure in this section is similar to the procedure introduced in [14]. In this section, the effect of different failure criteria and the usefulness of the stress correction factor were mainly investigated. The detailed model and simplified model for the dynamic impact analysis for the two interface bonding conditions are shown in Figure 12. A fuel rod with a length of 113.41 mm that included 10 pellets was used as a reference model to examine the dynamic response during the drop impact. The fuel rod segment was constrained to Zircaloy-4 blocks at both ends with a coupling constraint. The fuel rod and Zircaloy-4 block impact a rigid surface in the horizontal orientation, as shown in Figure 12.

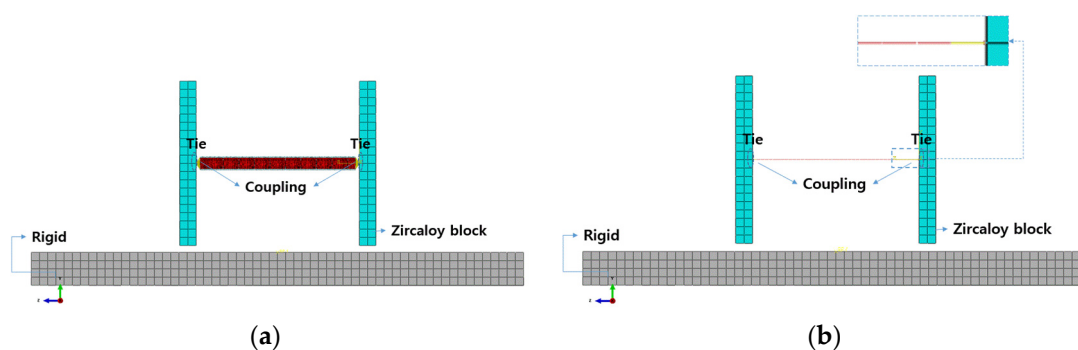


Figure 12. Finite element model for the dynamic analysis: (a) detailed model; (b) simplified model.

ABAQUS/Explicit was used for the dynamic impact simulations, and the drop heights in the range of 0.3 m to 1.5 m were transformed into the initial velocity using Equation (9) as follows:

$$v = \sqrt{2gh}, \quad (9)$$

where v is the initial velocity (mm/s); g is the gravitational acceleration (mm/s²), and h is the drop heights (mm).

4.2. Results and Discussion

Dynamic impact simulations were performed considering four drop heights for both of the interfacial conditions. The results of the maximum deflection of the beam and membrane plus bending stress are summarized in Tables 7 and 8. It was observed that the deviation of the maximum deflection of the detailed model and the simplified model is 9.9% for the fully bonded condition and 19.0% for the fully de-bonded condition. During impact, a shear force is exerted to the fuel rods and a bending moment resulting from the inertia of mainly the fuel pellets, and the fully de-bonded fuel rods have less shear resistance than that of the fully bonded fuel rods. It is believed to be the cause of the bigger

deviation of the deflection results in the fully de-bonded case, and its results are consistent with those reported in [14]. At the same drop height of 1 m, the maximum displacement deviation of the detailed model of the two interfacial bonding conditions is 25%, confirming that the PCI has a significant effect on the fuel rod behavior in a drop accident.

Table 7. Results of the dynamic analyses for the fully bonded condition.

No.	Drop Height (m)	Model	Max. Displacement		Correction Factor	Stress * ($\sigma^m + \sigma^b, \sigma_{vm}$)	
			Value (mm)	Dev. (%)		Value (MPa)	Dev. (%)
1	0.3	Detailed	0.42	9.9	1.78	437	62 (31)
		Simplified	0.46			168 (300)	
2	0.5	Detailed	0.54	5.0		674	59 (28)
		Simplified	0.57			274 (487)	
3	1.0	Detailed	0.80	3.3		697	55 (21)
		Simplified	0.85			308 (548)	
4	1.5	Detailed	0.99	8.4		757	58 (0.6)
		Simplified	1.16			423 (752)	

* Numbers in parenthesis are those corrected by multiplying by the correction factor.

Table 8. Results of the dynamic analyses for the fully de-bonded condition.

No.	Drop Height (m)	Model	Max. Displacement		Correction Factor	Stress * ($\sigma^m + \sigma^b, \sigma_{vm}$)	
			Value (mm)	Dev. (%)		Value (MPa)	Dev. (%)
1	0.3	Detailed	0.56	12.3	3.06	322	61 (18)
		Simplified	0.63			124 (379)	
2	0.5	Detailed	0.54	15.3		433	64 (9.0)
		Simplified	0.57			156 (478)	
3	1.0	Detailed	1.00	19.0		638	66 (4.2)
		Simplified	1.19			217 (664)	
4	1.5	Detailed	1.23	10.8		727	67 (0.1)
		Simplified	1.47			240 (734)	

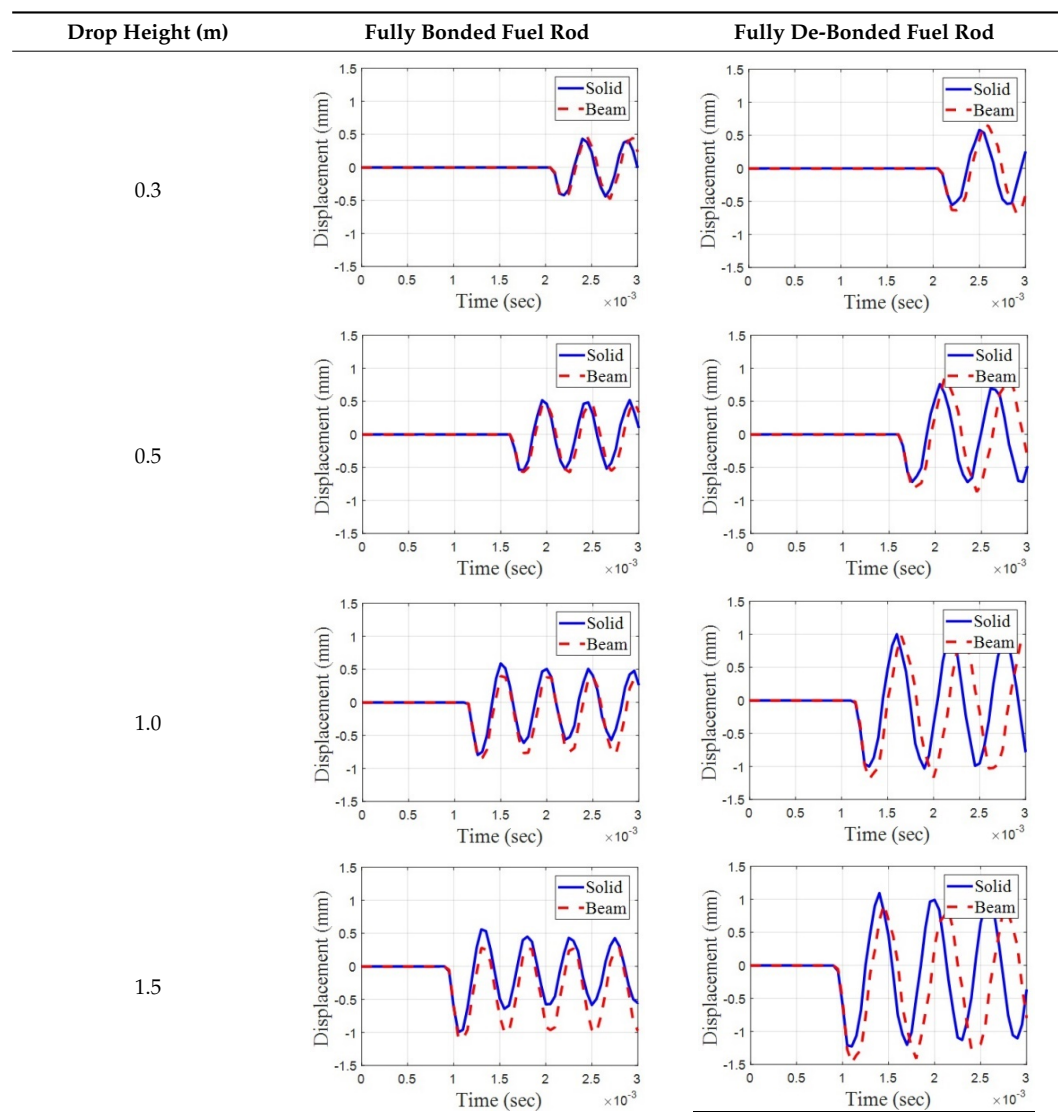
* Numbers in parenthesis are those corrected by multiplying by the correction factor.

The maximum membrane plus bending stresses during the impacts are summarized in Tables 7 and 8. The numbers in parenthesis are those corrected by multiplying the stress correction factor derived in Section 3 to the results of the simplified models. When the stress compensation factors were applied, the deviation of the stress predictions in the detailed model and the simplified model ranged up to 31% in the fully bonded case and up to 18% in the fully de-bonded case. However, those errors diminish to almost 0 as the drop height approaches the critical drop height, where the membrane plus bending stress becomes 749 MPa. For the fully bonded case, the critical drop height is predicted around 1.5 m, and for the fully de-bonded case, it is expected to be bigger than 1.5 m. It is very notable that the critical drop height is bigger in the fully de-bonded case than in the fully bonded case, which is different from the conclusions reported in other works [11,13,14].

One reason for this phenomenon is that the von Mises stress is used in the failure criteria for the stress linearization. The von Mises stress and the Tresca stress are governed by the shear component in a stress state and are suitable for the prediction of ductile failure. In the fully bonded condition, a much bigger shear stress is developed in the cladding within the vicinity of the pellet–clad interface than in the fully de-bonded case. Another reason is that the stress is more localized in the fully bonded case. Stress is concentrated in the narrow region around the pellet–pellet interface, which is relatively flexible compared to the other area of the cladding, which is bonded to the pellets. This is clearly seen in Figure 8. It can be seen that the stress is more uniformly distributed to the length of the cladding in the fully de-bonded case. The results of this section might be controversial, and it is believed that the failure criteria introduced in this study can be reasonably and conservatively applied to the prediction of cladding failure as long as its failure mechanism is a ductile failure. The validity of this statement can be checked if experimental data on fuel rod failure become available.

The deflection time history is summarized in Table 9. The solid lines with legend “solid” are the responses of the detailed model. It is seen that the simplified models are more flexible than the detailed model under the dynamic load, and this trend is more obvious in the fully de-bonded case. As discussed above, it is due to the difference in the shear resistance of the two interfacial conditions.

Table 9. History of the deflection of fuel rods calculated by dynamic impact simulations.



5. Discussion and Conclusions

In this study, a new failure criterion for SNF cladding was introduced. The membrane plus bending stress of the von Mises stress was used for the failure criterion, and the value is 749 MPa for the reference fuel rod considered in this work. The simplified beam models were developed based on parameter calibration using design optimization. The purpose of these models is to predict the failure of fuel rods in cask level analyses. To account for the effect of the PCMI, two separate models were developed for the fully bonded pellet–clad interface condition and the fully de-bonded interface condition. Because the beam models cannot simulate the concentrated stress state, stress correction factors were derived, which can be used in the prediction of the maximum membrane plus bending stress in the simplified models. The applicability of the simplified models and the stress correction factors were verified in the dynamic impact analyses, considering various drop heights. The following conclusions were drawn.

- In a comparison with the previous work of the authors, it is shown that the stress-based failure criterion is more conservative than the strain-based criteria based on the curvature of the deflected fuel rod.
- The stress correction factors are very effective in the failure prediction of the simplified beam models. However, the specific values of these factors can vary due to a number of factors, such as the shape of the fuel pellets, the material properties of the cladding and pellets, the gaps between the pellets and cladding, etc.
- In the dynamic impact simulations, the stress prediction using the simplified model and the stress correction factor show good accuracy as the drop height approaches the critical drop height. This is natural, because the simplified models were developed focusing on the failure point of the fuel rods.
- Although the fully bonded fuel rod deflects less than the fully de-bonded case, earlier failure is predicted with the stress-based failure criterion in the dynamic simulations. It is mainly due to the development of the shear stress in the interface of the fuel pellets and cladding in the fully bonded case. The validity of the failure criterion of the fuel cladding under a complicated 3D stress state should be confirmed with experimental data.
- The discrepancy of simplified model behavior can be reduced by adopting material models with more parameters to be calibrated together with more powerful fitting methods. It is expected that the correlation in the small loading situation can be improved significantly with such efforts.

Author Contributions: S.L. was the principal investigator of this research and contributed to the research planning, verification of the results and the manuscript writing. S.K. contributed to the survey of the relevant literature, scientific computing using ABAQUS and preparation of the data, figures and tables in the manuscript and the manuscript writing. All authors have read and agreed to the published version of the manuscript.

Funding: This work was funded by the Nuclear Safety Research Program through the Korea Foundation of Nuclear Safety (KoFONS) using the financial resource granted by the Nuclear Safety and Security Commission (NSSC) of the Republic of Korea (No. 2106042).

Conflicts of Interest: The authors declare no conflict of interest.

References

1. Ojovan, M.I.; Lee, W.E.; Kalmykov, S.N. *An Introduction to Nuclear Waste Immobilization*; Elsevier: Amsterdam, The Netherlands, 2019.
2. Lee, S.H.; Yook, D.S. Review of Spent Nuclear Fuel Dry Storage Demonstration Programs in US. *J. Nucl. Fuel Cycle Waste Technol.* **2017**, *15*, 135–149. [[CrossRef](#)]
3. U.S. Nuclear Regulatory Commission. *Licensing Requirements for the Independent Storage of Spent Nuclear Fuel, High-Level Radioactive Waste, and Reactor-Related Greater than Class C Waste, Rules and Regulations, Title 10, Part 72*; US NRC: Washington, DC, USA, 2010.
4. U.S. Nuclear Regulatory Commission. *Packaging and Transportation of Radioactive Material, Rules and Regulations, Title 10, Part 71*; US NRC: Washington, DC, USA, 2019.

5. IAEA Safety Standard. *Regulations for the Safe Transport of Radioactive Material*; Version 2021; Specific Safety Requirements No. SSR-6; IAEA: Vienna, Austria, 2012.
6. Choi, W.Y. Evaluation of Hydride Effect on Cladding Integrity under Spent Nuclear Fuel Dry Storage. Master's Thesis, Kyunghee University, Yongin, Korea, 2018.
7. Kang, Y.G. Degradation Evaluation of LWR Spent Nuclear Fuel for Dry Storage. Master's Thesis, Hanyang University, Seoul, Korea, 2019.
8. U.S. Nuclear Regulatory Commission. *Cladding Considerations for the Transportation and Storage of Spent Fuel, Interim Staff Guidance-11 Rev. 3*; US NRC: Washington, DC, USA, 2003.
9. Jiang, H.; Wang, J.A.; Wang, H. The impact of interface bonding efficiency on high-burnup spent nuclear fuel dynamic performance. *Nucl. Eng. Des.* **2016**, *309*, 40–52. [[CrossRef](#)]
10. Wang, J.A.; Wang, H.; Jiang, H.; Bevard, B. High burn-up spent nuclear fuel transport reliability investigation. *Nucl. Eng. Des.* **2018**, *330*, 497–515. [[CrossRef](#)]
11. Almomani, B.; Jang, D.; Lee, S. Structural integrity of a high-burnup spent fuel rod under drop impact considering pellet-clad interfacial bonding influence. *Nucl. Eng. Des.* **2018**, *337*, 324–340. [[CrossRef](#)]
12. Almomani, B.; Kim, S.; Jang, D.; Lee, S. Parametric study on the structural response of a high burnup spent nuclear fuel rod under drop impact considering post-irradiated fuel conditions. *Nucl. Eng. Technol.* **2019**, *52*, 1079–1092. [[CrossRef](#)]
13. Lee, S.; Kim, S. Simplified beam model of high burnup spent fuel rod under lateral load considering pellet-clad interfacial bonding influence. *Nucl. Eng. Technol.* **2019**, *51*, 1333–1344. [[CrossRef](#)]
14. Lee, S.; Kim, S. Development of equivalent beam model of high burnup spent nuclear fuel rods under lateral impact loading. *Metals* **2020**, *10*, 470. [[CrossRef](#)]
15. Kim, K.; Jang, Y.; Kim, J. In-Reactor Performance of an advanced PWR Fuel, PLUS7, for OPR1000s in Korea. *Nucl. Sci. Technol.* **2008**, *45*, 836–849. [[CrossRef](#)]
16. Geelhood, K.J.; Beyer, C.E.; Luscher, W.G. *PNNL Stress/Strain Correlation for Zircaloy (PNNL-17700)*; Pacific Northwest National Laboratory: Washington, DC, USA, 2008.
17. Adkins, H.; Geelhood, K.; Koeppl, B.; Coleman, J.; Bignell, J.; Flores, G.; Wang, J.A.; Sanborn, S.; Spears, R.; Klymyshyn, N. *Used Fuel Disposition Campaign, Used Nuclear Fuel Loading and Structural Performance under Normal Conditions of Transport—Demonstration of Approach and Results on Used Fuel Performance Characterization (FCRD-UFD-2013-000325)*; U.S. Department of Energy: Washington, DC, USA, 2013.
18. U.S. Nuclear Regulatory Commission. *A Pilot Probabilistic Risk Assessment of a Dry Cask Storage System at a Nuclear Power Plant (NUREG-1864)*; US NRC: Washington, DC, USA, 2010.
19. EPRI. *Spent Fuel Transportation Applications Assessment of Cladding Performance: A Synthesis Report (EPRI 1015048)*; Electric Power Research Inst.: Palo Alto, CA, USA, 2007.
20. EPRI. *Fuel-Assembly Behavior under Dynamic Impact Loads Due to Dry-Storage Cask Mishandling (EPRI-NP—7419)*; Electric Power Research Inst.: Palo Alto, CA, USA, 1991.
21. Choi, W.; Kim, T.; Seo, K. Shape optimization of a torus seal under multiple loading conditions based on the stress categories in the ASME code section III. *Nucl. Eng. Des.* **2011**, *241*, 2653–2659. [[CrossRef](#)]
22. Michael, S. *ABAQUS/Standard User's Manual*; Version 6.9; Dassault Systèmes Simulia Corp: Providence, RI, USA, 2009.
23. Li, H.; Ding, Q.; Huang, X. A New Method of Stress Linearization for Design by Analysis in Pressure Vessel Design. *Appl. Mech. Mater.* **2014**, *598*, 194–197. [[CrossRef](#)]
24. Bratton, R.; Jessee, M.; Wieselquist, W. *Rod Internal Pressure Quantification and Distribution Analysis Using FRAPCON (FCRD-UFD-2015-000636)*; US Department of Energy: Washington, DC, USA, 2015.
25. Velden, A.; Koch, P. Isight Design Optimization Methodologies. In *ASM Handbook Volume 22B, Metals Process Simulation*; Furrer, D.U., Semiatin, S.L., Eds.; ASM International: Geauga County, OH, USA, 2010.
26. Ingber, L. Adaptive Simulated Annealing (ASA): Lessons learned. *Control Cybern.* **1996**, *25*, 33–54.